Multifractal structure and Gutenberg-Richter parameter associated with volcanic emissions of high energy in Colima, México (years 2013-2015)

Marisol Monterrubio-Velasco[1], Xavier Lana[2], Raul Arámbula-Mendoza[3]

5

[1] Department of Computer Applications of Science and Engineering, Barcelona Supercomputing Center, Barcelona, 08034, Spain

[2] Department of Physics, ETSEIB, Universitat Politècnica de Catalunya, Diagonal 647, 08028 Barcelona, Spain

[3] Centro Universitario de Estudios e Investigaciones de Vulcanología (CUEIV), Universidad de Colima, Colima, 28045,
10 Mexico

Correspondence to: Marisol Monterrubio-Velasco (marisol.monterrubio@bsc.es)

Abstract. The evolution of multifractal structures in physical processes, for instance, climatology, seismology or volcanology, contributes to detecting changes in the corresponding phenomena. The evolution of the multifractal structure of volcanic emissions of low, moderate, and high energy (Colima, México years 2013-2015) contributes to this research to
15 detect quite evident signs of the immediacy of possible dangerous emissions of high energy close to 8.0×10^8 J. These signs are manifested by the evolution of six multifractal parameters: the central Hölder exponent (α_0), the maximum and minimum Hölder exponents (α_{max}, α_{min}) the multifractal amplitude ($W = \alpha_{max} - \alpha_{min}$), the multifractal asymmetry ($\gamma = [\alpha_{max}-\alpha_0]/[\alpha_0-\alpha_{min}]$) and the complexity index, CI, which is defined as the addition of normalised values of α_0, W and γ. The results of the adapted Gutenberg-Richter seismic law to volcanic emissions of energy, as well as the corresponding skewness and standard
20 deviation of the volcanic emission data, also contribute to confirming the results obtained using multifractal analysis. The obtained results, based on multifractal structure, adaptation of Gutenberg-Richter law to volcanic emissions, and basic statistical parameters, could be assumed as relevant to prevent a forthcoming volcanic episode of high energy, which could be additionally quantified by an appropriate forecasting algorithm.

1 Introduction

25 The fractal and multifractal theory applied to Earth sciences (Goltz, 1997; Turcotte, 1997 and Karsten et al., 2005, among many others) could be an interesting contribution to analyse the complex geophysics and atmospheric mechanisms, as well as a relevant step on a forecasting process. Some examples could be, for instance, the rainfall regimes (Koscielny-Bunde et. al, 2006 and Lana et al., 2017, 2020, 2023) the extreme temperature structures (Burgueño et al., 2014) the wind speed characteristics (Feng, 2009), hydrological analysis (Movahed M. S. and Hermanis E., 2008) and the seismic activity (Gosh et

30 al., and 2012; Telesca and Toth 2016 and Monterrubio-Velasco et al., 2020) and emissions of volcanic energy (Monterrubio-Velasco et al., 2023).

The forecasting of volcanic energy emissions, from the point of view of monofractal theory (Hurst exponent and Reconstruction theorem) (Diks, 1999) and predictive algorithms and nowcasting processes (Rundle et al., 2016) could prevent imminent dangerous episodes. An example of monofractal theory is the analysis of the series of volcanic emissions

35 in Colima (México), years 2013-2015 (Arámbula-Mendoza et al., 2018, 2019; Monterrubio-Velasco et al., 2023) which, together with the mentioned concept of nowcasting, determine a probable level of volcanic energy for the next emissions. A quite different strategy is based on multifractal theory (Kantelhardt et al. 2002), which has been also applied in seismology (Shadkhoo and Jafari, 2009 and Telesca and Toth, 2016, among others) and climatology (Mali, 2014 and Lana et al., 2016, 2017, among others).

40 One of the most relevant law in seismology, the Gutenberg-Richter equation (Gutenberg and Richter, 1944), describes the earthquake frequency-magnitude distribution for local, regional or global seismic sequences:

$$\log_{10} N = a - b\, M_w \tag{1}$$

45 N represents the cumulated number of events exceeding a magnitude M_w and the parameter b, usually called b-value, is associated with the reduction of the number earthquakes for increasing values of the seismic magnitude. The b-value is also related to the differential stress of the Earth's crust: highly stressed zones, or faults, usually exhibit low b-values, whereas weakly stressed areas usually exhibit higher b-values (Scholz, 2015). Gulia and Wiemer, (2019) suggest that a decrease in b-value on the mainshock's fault can indicate that the strongest event of the sequence has not yet occurred, being this

50 information useful to forecast future stronger earthquakes. For these reasons, analysing the time series of the b-value can be a powerful tool to enhance seismologist forecasting capability (Taroni et al., 2021).The Gutenberg-Richter equation is also useful for the analysis of volcanic emissions bearing in mind the seismic moment magnitude, M_w, is related to the emission of seismic energy, E_s, by means of the power law (Kanamori, 1977)

55 $$M_w = 2/3 \log E_s - 3.2 \tag{2}$$

Therefore, it is possible to apply in the present research an equivalent GR law to the energy of volcanic explosions series in Volcán de Colima, substituting seismic magnitudes by the logarithm of the volcanic energy emissions E.

60 $$\log_{10} N = b \log_{10} E + a \tag{3}$$

The objective of this research is not forecasting the magnitude of the next emission (forecasting or nowcasting strategy), but verifying that a specific evolution of a set of multifractal parameters, based on the successive analysis of data segments, would manifest the vicinity of a future real extreme energetic emission. It is also relevant that the results obtained from the

65 viewpoint of the multifractality are in agreement with the evolution of the b-value when the segments of volcanic emissions are approaching to the extreme emission of energy.

The second section, Database, details the basic characteristics of the complete set of emissions and justifies the database quality. The third section, Multifractal Theory, is divided into three parts, corresponding to, first, a detailed description of the multifractal detrended fluctuation theory, second, the multifractal spectrum and, third, the complexity index. The fourth

70 section, Evolution of the Multifractal Parameters, depicts the characteristics of all the multifractal parameters detecting the vicinity to an extreme emission of volcanic energy. The fifth section, Gutenberg-Richter evolution, ~~contributes to confirm~~ the vicinity of an extreme emission of energy ~~based on~~ changes of the b parameter. Finally, the sixth section summarises the results obtained, being also discussed the degree of applicability of this strategy and the comparison with forecasting and nowcasting processes.

75 **2 Database**

~~The~~ series of volcanic explosions, also known as Vulcanian ~~explosions~~ (Bachtell Clarke and Esposti Ongaro, 2015) emitted by Volcán de Colima (Western segment of Trans-Mexican volcanic belt, years 2013-2015) (Arámbula-Mendoza et al., 2018, 2019) ~~are chosen~~ to analyse, from the point of view of the multifractal theory, the imminence of emissions associated with energies close to or exceeding 10^8 Joules. Fig. 1 depicts the emissions accomplishing the Gutenberg-Richter law, consisting

80 in 6182 data with energy equalling to or exceeding approximately 2×10^6 J within the interval of years 2013-2015. The most relevant energy emissions are detected just at the beginning of the recorded data [log10 (Energy) =8.2], approximately at the middle of the series [log10 (Energy) = 8.4] and at the end of the series [log10 (Energy) = 8.5]. A more detailed description of the volcanic emission based on the Generalised Logistic Distribution (GLO), based on L-moments theory (Hosking and Wallis, 1997) and expected values

85

for return periods corresponding to extreme emissions with 90, 95 and 99% of probability, determined by the Generalised Extreme Values distribution (GEV), also based on L-moments distribution, can be found in Monterrubio-Velasco et al. (2023), where can be observed that the highest extreme emissions with probability 90% exceed an energy level of log10 (Energy) = 8.0.

90

As mentioned, two of the three maximum emissions are detected at the beginning and at the end of the dataset, being not possible to respectively complete the evolution of the multifractal parameters before and after these two extreme emissions. The research is finally applied to the emission of [log10 (Energy) 8.4] with a detailed analysis applied to successive moving

Nonlinear Processes
in Geophysics
Discussions

Open Access

EGU

95 windows with a length of 1000 data (sufficient for a right analysis of multifractality) and a shift of 100 data, being obtained in this way 27 samples of the evolution of the different parameters describing the proximity to the highest emission. Fig. 2 depicts this evolution of the energy since the emission 1500 up to 3000, with minimum, average and maximum energy emissions respectively close to log10(Energy) equal to 6.3, 6.6 and 8.4. Consequently, the maximum energy exceeds one hundred times the average energy of this emissions segment.

3 Multifractal methodology

3.1 Multifractal Detrended Fluctuation Anaysis (MF-DFA)

The analysis of multifractal properties in nonstationary series can be approach by employing the multifractal detrended fluctuation analysis (MF-DF) technique, as introduced by Talkner and Weber (2000). A comprehensive description of the

105 MF-DF methodology can be found in the work by Kantelhardt et al. (2002). Following the MF-DF is summarize. Considering {xk} as a time series with a length of N, the algorithm's steps are:

A. Computing the 'profile' of the time series as

$$Y(i) = \sum_{k=1}^{i} x_k - \langle x \rangle, i = 1, \ldots, N \ , \tag{4}$$

110

where $< x >$ is the average value of the {xk}.

B. Dividing $Y(i)$ into $N_s = int(N/s)$ non-overlapping segments of equal length s. Considering that the length N of the series is often not a multiple of the considered segment lengths, a short part at the end of the profile would be discarded. With the aim of not disregarding this part of the series, the same procedure is repeated starting from the opposite end. Consequently, $2N_s$

115 segments are obtained.

C. Computing the local variance $F^2(s,u)$ for every segment u of length s by using a four order least-square polynomial fitting to obtain the differences between "profile" segments (first step) and the corresponding polynomial fitting.

D. Calculating the q-order fluctuation function:

$$F(s)_q = \left[\frac{1}{2N_s} \sum_{1}^{2N_s} \ln\left(F^2(s,v)\right)^{q/2} \right]^{1/qv}, q \neq 0 ; -\infty < q < +\infty \tag{5}$$

120 $$F(s)_0 = \left[\frac{1}{4N_s} \sum_{1}^{2N_s} \ln\left(F^2(s,v)\right) \right], q = 0 \tag{6}$$

The steps 2, 3 and 4 must be repeated for several scales *s*, it is appropriate that these scales vary within the range (*m*+2, *N*/4), where m =4 the chosen polynomial order (third step).

E. The q-order fluctuation function is anticipated to exhibit a power-law relationship concerning the segment length, *s.*:

$$F(s)_q \approx s^{h(q)}$$ (7)

125 and *h(q)*, the generalized Hurst exponent, can be determined by a linear regression of $\ln\{F(S)_q\}$ versus $\ln(s)$.

In the case of non-stationary series, such as fractal Brownian signals, the exponent $h(q = 2)$ will be larger than 1.0 and will satisfy $h(2) = H + 1$, where H is the well-known Hurst exponent (Movahed and Hermanis, 2008). For stationary time series, the value $h(q = 2)$ is identical to the Hurst exponent. $H > 0.5$ indicates persistence in long-range correlation, $H \approx 0.5$ manifests the random character of the series, while $H < 0.5$ reflects anti-persistence. In the case of multifractal series, if positive values

130 of q are considered, the segments ν with large variance (i.e. large deviations from the corresponding polynomial fit) will dominate the *Fq(s)* average. Thus, for positive values of *q*, *h(q)* corresponds to the scaling behavior of the segments with large fluctuations. For negative values of *q*, the segments ν with small variance $F^2(s,v)$ will dominate the *Fq(s)* average, *h(q)* then describing the scaling behavior of the segments with small fluctuations (Movahed and Hermanis, 2008; Burgueño et al., 2014).

135 **3.2 The Singularity Spectrum**

The singularity spectrum, f(α), is related to the generalized Hurst exponent h(q) through of the Legendre transform (Kantelhardt et al., 2002). This relationship is articulated as follows:

$$\alpha = h(q) + q\frac{dh(q)}{dq} \leftarrow Legendre\ Transfrom \rightarrow f(\alpha) = q[\alpha - h(q)] + 1$$ (8)

where α is the singularity strength or Hölder exponent, and *f(α)* denotes the dimension of the subset of the series. The

140 multifractal scaling exponent, also is known as mass exponent, is

$$\tau(q) = qh(q) - 1$$ (9)

and the Hölder exponent is defined as

145 $$\alpha(q) = d\tau(q)/dq$$ (10)

The function f(α) describes the subset dimension of the series characterized by the same singularity strength α, with the singularity strength with maximum spectrum designed as α_0. Small values of α_0 mean that the underlying process loses fine-structure, that is, becomes more regular in appearance; conversely, a large value of α_0 ensures higher complexity. The shape

150 of f(α) may be fitted to a quadratic function around the position α_0

$$f(\alpha) = A(\alpha - \alpha_0)^2 + B(\alpha - \alpha_0) + C$$ (11)

The coefficient B manifests the asymmetry of the spectrum, being null for a symmetric spectrum. A right-skewed spectrum, $B > 0$, indicates fine structure, while left-skewed shapes, $B < 0$, point to smooth structure. The width of the spectrum, W, can

155 be obtained by extrapolating the fitted curve $f(\alpha)$ to zero or, in other words, extrapolating the multifractal spectrum to $q \rightarrow \pm \infty$. The spectral amplitude is defined as

$$W = \alpha_{max} - \alpha_{min} \tag{12}$$

with $f(\alpha_{max}) = f(\alpha_{min}) = 0$ and $\alpha_{max}\ q \rightarrow -\infty$ being larger than $\alpha_{min}\ q \rightarrow +\infty$. Given that q uses to be chosen many times ranging, for instance, within the (-15, +15) interval, α_{max} and α_{min} have been obtained by numerically extrapolating the Eq.

160 (11) to $f(\alpha) = 0$.

The multifractal parameters used to detect the evolution towards an extreme energy emission could be α, the Hölder exponent. More concretely, the central Hölder exponent, α_0, and the extreme Hölder exponents, α_{max} and α_{min}, respectively accomplishing $f(\alpha_0) = 1.0$ and $f(\alpha_{max}) = f(\alpha_{min}) = 0$. The multi-spectral amplitude W (Eq. 12) and the multifractal asymmetry

165 $$\gamma = \frac{\alpha_{max} - \alpha_0}{\alpha_0 - \alpha_{min}} \tag{13}$$

also contribute to detect the vicinity of an extreme emission. All these parameters could be combined in a single the complexity index, CI, defined in Shimizu et al. (2002):

$$CI(j) = \left[\alpha_0(j) - \frac{\langle \alpha_0 \rangle}{\sigma(\alpha_0)} \right] + \left[W_j - \frac{\langle W \rangle}{\sigma(W)} \right] + \left[\gamma_j - \frac{\langle \gamma \rangle}{\sigma(\gamma)} \right] \tag{14}$$

170 where $j=1,..,N$ representing the N data segments for which the multifractal spectrums is computed and $\langle * \rangle$ and $\sigma(*)$ the corresponding average and standard deviation per each parameter calculated in the N samples. The evolution of every multifractal parameter close to the extreme emission of energy will be clearly decreasing or increasing depending on every one of the specific parameters (α_0, α_{max}, α_{min}, W and γ), then affecting the global CI

175 **4. Results**

4.1 Evolution of the multifractal parameters

The evolution of the multifractal parameters is analysed applying the multifractal detrended fluctuation analysis algorithm, MDFA, to 27 moving windows (MWs) data of length 1000 elements (sufficient to obtain accurate multifractal analyses) and

180 shift of 100 elements. In this way, the multifractal structure is analysed from the beginning of the available data series up to a notable number of volcanic energy emissions after the extreme energy E, given in units of Joule, which is close to $\log 10 E = 8.4$. A first point of view of the evolution of the multifractal structure is depicted in Fig. 3, where neither the first four moving windows (before the highest emission) nor the two last (after the highest emission) include the emission of the

mentioned extreme energy. A simple review of the multifractal structure is not sufficient to detect the vicinity to the highest
185   emission, given that a good fit of the empiric values of multifractality to a theoretical 2nd degree polynomial structure does
not imply vicinity to an extreme maximum emission. Nevertheless, the Hölder exponents, describing different multifractal
amplitudes and asymmetries for every moving window suggest an alternative to detect the vicinity to the highest emission.

Fig. 4 describes the evolution of the Hölder parameter characteristics (α_0, α_{max}, α_{min}, W) for the 27 moving windows. Bearing
in mind that the highest emission is included since the MW number 16 up to the number 25, the most relevant results ~~could~~
190   ~~be~~:

   a) An increasing tendency of amax, with some fluctuations before MW-15 and a clear decrease after the emission of the
highest energy (MW-16).

   b) Some fluctuation of amin up to MW-16 and a fast increase after this MW.

   c) A clear decrease of α_0 arriving to MW-15, with a notable increase for some of the next MWs including the highest
195   emission.

   d) A clear maximum of W for MW-16 and also evident increasing and decreasing evolutions, respectively before and after
MW-16.

Additionally, Fig. 5 depicts the evolution of the Hurst exponent, h(q=2), the multifractal asymmetry, γ, and the complexity
index, CI. The corresponding characteristics are:

200   e) A quite similar structure of the Hurst exponent (h(q=2) in comparison with the evolution of α_0.

   f) An evolution of the asymmetry γ quite similar to ~~W~~ .

   g) An evolution of CI quite similar to ~~W~~.

All the seven multifractal parameters depict some characteristic changes close to, previously or after ~~the MW including the~~
~~highest emission~~, but the Complexity Index, CI, ~~should~~ be the best premonitory of a highest emission of energy.
205   Additionally, the Hurst exponent, h(q=2), is characterised by the highest prevalence of randomness, h(q=2) ~ 0.5, for the
MWs including the highest emission, quite different to h(q=2) ~ 0.60 – 0.65, obtained for the other MWs, with prevalence of
moderate persistence.

Another ~~point of view to detect~~ the immediacy of a high energy emission could be based on the evolution of the parameter
$\tau(q) = qh(q) - 1$. Fig. 6 depicts six examples of MWs (the first three not including the highest emission and the other three
210   including it). As expected and justified by the mathematical theory of the Multifractal algorithm, the change of the dt(q)/dq
is always detected in q = 0 and the corresponding square regression coefficients of both linear evolutions are very close to
1.0. ~~Fig. 7 describes the evolution of the two dτ(q)/dq for the MWs number 9 to 19, being only noticeable the small negative~~
~~trend of dτ (q)/dq for q>0 and previous to the MW16.~~

215   **4.2 Evolution of the Gutenberg-Richter ~~parameter~~ for volcanic emissions**

7

The results obtained by means of the multifractal theory are complemented by analysing the evolution of ~~the parameter~~ b of the Gutenberg-Richter law adapted to volcanic emission of energy (Eq. 3), with the aim of detecting changes on this parameter along the 27 MWs. The 1000 consecutive emissions of energy for every MW are assumed to be sufficient to

220 correctly determine b, with small uncertainty, for every MW. The minimum acceptable log10(E) = 6.3 for every MW is also assumed to be the same obtained for the whole series of volcanic emissions (Fig. 1). The evolution of the ~~parameter b~~, together with standard deviation and skewness of the log10E for the different MWs, is represented in Figs. 8a, 8b and 8c. First of all, the decreasing trend of approximately 0.27 units of b for every MW since MW11 to MW16 is notable, being also relevant that the Gutenberg-Richter parameter for the whole series ($b = 3.84$, Fig. 1) and for the MW16, the first Moving

225 Window including the highest emission ($b = 4.191$), are relatively similar. Additionally, the standard deviation of log10E corresponding to MW16 (0.273) is also remarkably similar to that corresponding to the whole series (0.283) and a clear increment of log10E dispersion (standard deviation) is observed for the consecutive MWs approaching to the extreme emission. Something similar is detected for the skewness, with a value of 1.394 (the whole series) and of 1.359 (MW16), as well as a clear increment of the skewness approaching to the first MW including the extreme volcanic energy emission. In

230 short, from the point of view of the Gutenberg-Richter ~~parameter~~ and two basic statistical ~~parameters~~ (standard deviation and skewness), these three factors could also contribute to confirm the evolution towards a volcanic emission of extreme energy.

5. Conclusions

The analysis of the complexity and possible forecasting of volcanic emissions of energy, previously analyzed from the point

235 of view of the reconstruction theorem, have been now ~~basically~~ analyzed in this ~~research~~ by means of the multifractal theory, with additional ~~concepts~~ based on the evolution of the ~~Gutenberg-Richter b parameter~~ and two basic statistical ~~definitions~~ (standard deviation and skewness). The obtained results permit a better understanding of the complex physical mechanisms governing these geophysical phenomena, without forget the nowcasting (based on statistics) and forecasting algorithms (based on predictive algorithms and the reconstruction theorem).

240 It is relevant to remember that the main objective of this research is not an accurate forecasting of every volcanic emission of energy, but the detection of the best parameters with evolutions manifesting signs of a probable imminence of an emission of extreme energy. In spite of the best parameter could be the complexity index, CI, based on the multifractal parameters α_0, W and γ, the evolution of every one of the multifractal parameters, as well as of the Gutenberg-Richter parameter b and the standard deviation and skewness of the emitted volcanic energy (all of them obtained for every one of the moving windows),

245 should be also considered for a better detection of a forthcoming extreme emission.

In spite of the ~~facilities~~ offered by the multifractal parameters, the Gutenberg-Richter law and the standard deviation and skewness to detect possible forthcoming extreme emissions, the step by step forecasting of every emission (~~bearing in mind the~~ appropriate algorithms and the results of the reconstruction theory) should be also relevant to complement the control of these emissions. ~~By one hand, the results obtained in this research depict that the evolution of several parameters detects that~~

250 ~~an extreme emission is being generated~~. On the other hand, a forecasting algorithm could determine step by step, ~~but~~ with

some level of uncertainty, the ~~values~~ of ~~the~~ consecutive emissions. For example, an emission of log10(E) = 7.52, relatively close to the extreme one, is approximately recorded 17 days before. The other three high emissions {log10(E) = 7.84, 7.71 and 7.65} are detected just a day or a few hours before the cited extreme emission. Remembering the foreshock concept in seismology, these four high emissions could be the "foreshocks" of the expected extreme emission. Nevertheless, whereas

255 the first cited high emission, log10(E) = 7.52, could be a warning of 17 days before the extreme emission, the other three high emissions are detected only a few hours before the extreme episode. Conversely, the warning parameters proposed in this ~~research~~ detect signs of a forthcoming extreme energy emission a notable number of days before. A good example is the evolution of the Complexity Index, CI, which clearly increases since MW6 to MW11 (interval close to 100 days) and oscillates since MW12 to MW15 (close to 90 days before the extreme emission).

260 In short, multifractal structures theory, basic statistical parameters and the Gutenberg-Richter law for a set of MWs, together with an appropriate forecasting algorithm based on the reconstruction theorem, could represent a notable improving on the predictability of high volcanic energy emissions with a long enough time interval of days to prevent or mitigate the effects of these volcanic emissions.

Competing interests

265 The contact author has declared that none of the authors has any competing interests

275 **References**

Arámbula-Mendoza, R., Reyes-Dávila, G., Vargas-Bracamontes, D. M., González-Amezcua M., Navarro-Ochoa, C., Martínez-Fierros, A., Ramírez-Vázquez, A. Ariel.: Seismic monitoring of effusive-explosive activity and large lava dome collapses during 2013–2015 at Volcán de Colima, Mexico. Journal of Volcanology and Geothermal Research, 351, 75-88, 2018.

280

Arámbula-Mendoza, R., Reyes-Dávila, G., Domínguez-Reyes, T., Vargas-Bracamontes, D., González-Amezcua, M., Martínez-Fierros, A., Ramírez-Vázquez, A.: Seismic Activity Associated with Volcán de Colima. In Volcán de Colima, portrait of a Persistently Hazardous Volcano. Ed. Springer, 2019.

285 Bachtell Clarke, A., Esposti Ongaro, Belousov T.: Vulcanian eruptions. The Encyclopedia of Volcanoes, Editor in chief, Haraldur Sigurdsson. Elsevier, 2015.

Nonlinear Processes
in Geophysics
Discussions
Open Access

EGU

Burgueño A., Lana X., Serra C., Martínez M.D.: Daily extreme temperature multifractals in Catalonia (NE Spain). Physics Letters A, 378, 874-885, 2014.

290

Diks, C.: Nonlinear time series analysis. Methods and Applications. Nonlinear Time Series and Chaos (4). World Scientific, 209 pp.10, 1999.

Feng T., Zuntao Fu Z., Deng X., Mao J. (2009): A brief description to different multi-fractal behaviours of daily wind speed
295 records over China. Physics Letters A 373, 4134–4141.

Ghosh D., Dep A., Dutta S., Sengupta R., Samanta S.: Multifractality of radon concentration fluctuation in earthquake related signal. Fractals, 20, 33-39, 2012.

300 Goltz, Ch.: Fractal and chaotic properties of earthquakes. Lecture Notes in Earth Sciences (77), 178 pp, Springer-Verlag, Berlin, 1997.

Gulia, L. and Wiemer, S.: Real-time discrimination of earthquake foreshocks and aftershocks. Nature, 574, 193–199, 2019.

305 Gutenberg, B. and Richter, C. Frequency of earthquakes in California. Bull. Seismol. Soc. Am. 34, 185–188, 1944.

Hosking, J.R.M. and Wallis, J.R.: Regional Frequency Analysis. An approach based on L-Moments. Cambridge University Press, New York, 224 pp, 1997.

310 Kanamori, H.: The energy release in great earthquakes. Journal of Geophysical Research, 82 (20): 2981–2987, doi:10.1029/jb082i020p02981, 1977.

Kantelhardt J.W., Zschiegner S.A., Koscielny-Bunde E., Havlin S., Bunde A., Stanley H.E.: Multifractal detrended fluctuaction analysis of nonstationary time series. Physica A, 316, 87-114, 2002.
315

Karsten, B., Dimri, V.P., Maurizio, F.,Donato, F. Hiaso, I., Yasuto, K., La Manna, M., Lapenna, V., Pervukhina, M., Srivastava, H.N., Srivastava, R.P., Surkok, V.V., Tanaka, H., Telesca, L. Vedanti, N.: Fractal behaviour of the Earth system. Dimri, V.P. Editor. Springer-Verlag, 205 pp, 2005.

320 Koscielny-Bunde E., Kantelhardt J.W, Braund P., Bunde A., Havlin S.: Long-term persistence and multifractality of river runoff records: Detrended fluctuation studies. Journal of Hydrology 322,120–137, 2006.

Lana, X., Burgueño, A., Martínez, M.D., Serra, C.: Complexity and predictability of the monthly western Mediterranean oscillation index. International Journal of climatology, 36, 2435-2450, doi 10.1002/joc.4503, 2016.

325

Lana, X., Burgueño, A., Serra, C., Martínez, M.D.: Multifractality and autoregressive processes of dry spell lengths in Europe: an approach to their complexity and predictability. Theoretical and Applied Climatology, 127, 285-303. DOI 10.1007/s00704-015-1638-0, 2017.

330 Lana, X., Rodríguez-Solà, R., Martínez, M.D., Casas-Castillo, M. C., Serra, C., Kirchner,R.: Multifractal structure of the monthly rainfall regime in Catalonia (NE Spain): Evaluation of the non-linear structural complexity of the monthly rainfall. CHAOS: Interdisciplinary Journal of Nonlinear Science, 30(7). DOI: 10.1063/5.0010342, 2020.

Lana, X., Casas-Castillo, M.C., Rodríguez-Solà, R., Prohoms, M., Serra, C., Martínez, M.D., Kirchner, R.: Time trends,
335 irregularity, multifractal structure and effects of CO2 emissions on the monthly rainfall regime at Barcelona city, NE Spain, years 1786-2019. International Journal of Climatology, https://doi.org/10.1002/joc.7786, 2023.

Monterrubio, M., Lana, X., Arámbula-Mendoza, R.: Uncertainties, complexities and possible forecasting of the volcán de Colima energy emissions (Mexico, years 2013-2015) based on the fractal reconstruction theorem. Nonlinear Process in
340 Geophysics (In press). https://doi.org/10.5194/egusphere-2023-1153, 2023.

Mali P.: Multifractal characterization of global temperature anomalies.Theoretical and Applied Climatology. DOI 10.1007/s00704-014-1268-y, 2014.

345 Monterrubio-Velasco, M., Lana, X., Martínez, M.D. Zúñiga, R. and de la Puente, J.: Evolution of the multifractal parameters along different steps of a seismic activity. The example of Canterbury 2000-2018 (New Zealand). AIP Advances. DOI: 10.1063/5.0010103, 2020.

Movahed M. S. and Hermanis E.: Fractal analysis of river flow fluctuations. Physica A, 387, 915–932, 2008.
350 Rundle, J.B., Turcotte, D.L., Donnellan, A., Grant, Ludwig, L., Luginbuhl, M., Gong, G.: Nowcasting earthquakes. AGU Publications. https://doi.org/10.1002/2016EA000185, 2016 .
Shadkhoo, S. and Jafari, G.R.: Multifractal Detrended Cross-Correlation Analysis of Temporal and Spatial Seismic Data. The European Physical Journal B, 72, 679-683, https://doi.org/10.1140/epjb/e2009-00402-2, 2009.

355 Shimizu Y., Thurner S., Ehrenberger K.: Multifractal spectra as a measure of complexity in human posture. Fractals, 10, 103-116, 2002.

Scholz, C.H.: On the stress dependence of the earthquake b value. Geophys. Res. Lett.. 42, 1399 –1402, 2015.

360 Talkner, P., Weber, R.O.: Power spectrum and detrended fluctuation analysis: Application to daily temperatures. Physical Review E 62, 150, 2000.

Taroni, M., Vocalelli, G., De Polis, A.: Gutenberg–Richter b-value Time Series Forecasting: A Weighted Likelihood Approach. Forecasting, 3, 561-569. https://doi.org/10.3390/forecast3030035, 2021.
365
Telesca, L. and Toth, L.: Multifractal detrended fluctuation analysis of Pannonian earthquakes magnitude series. Physica A, 448, 21-29, 2016.

Turcotte, D.L.: Fractals and Chaos in Geology and Geophysics. Cambridge University press (2nd edition), 398 pp., 1997.
370

375
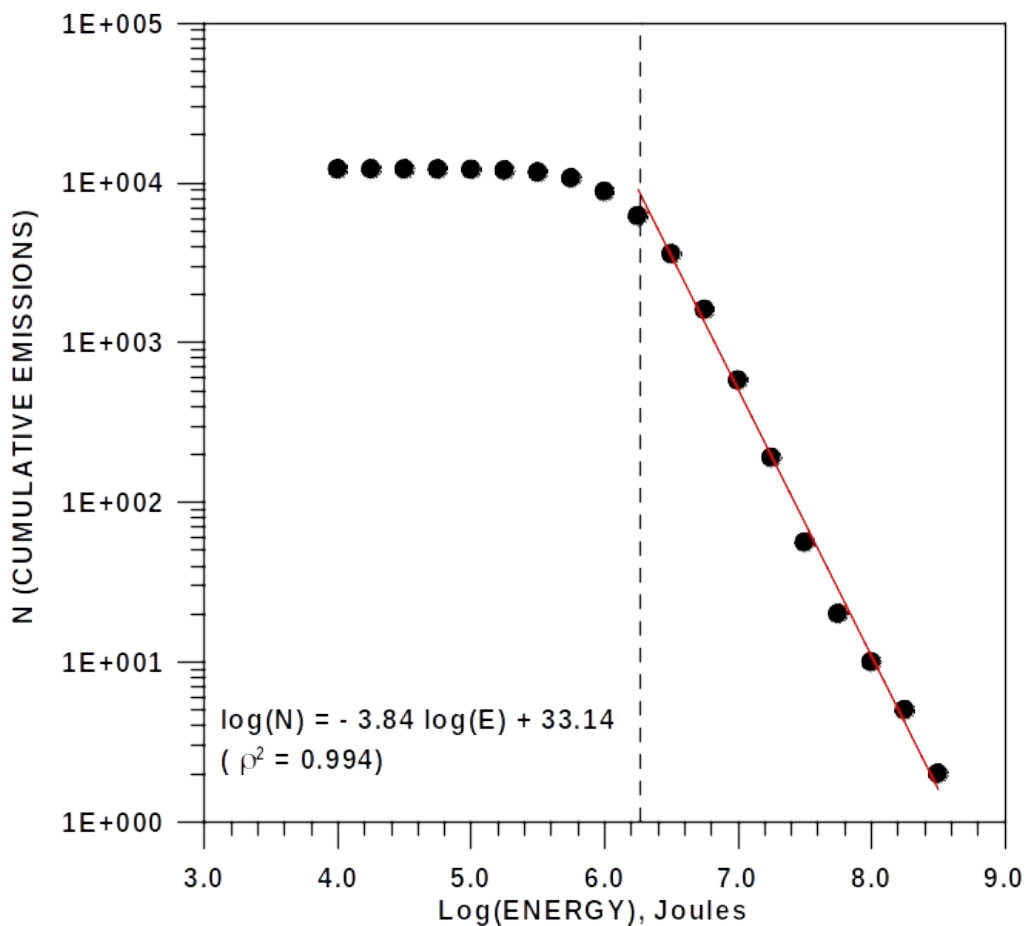
Figure 1: Volcanic emissions of energy (Joules) exceeding log10(E) = 6.1 and accomplishing the Gutenberg-Richter

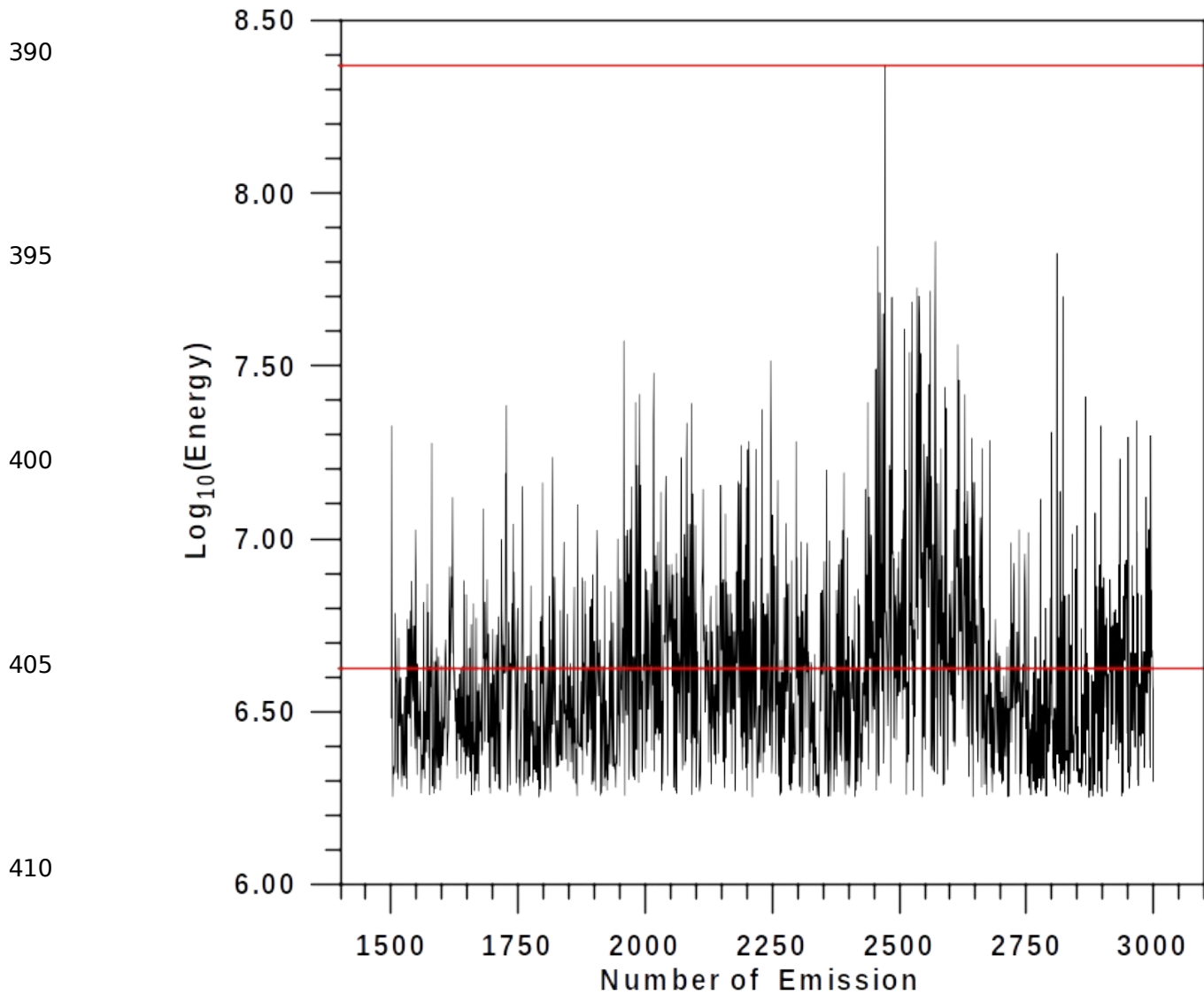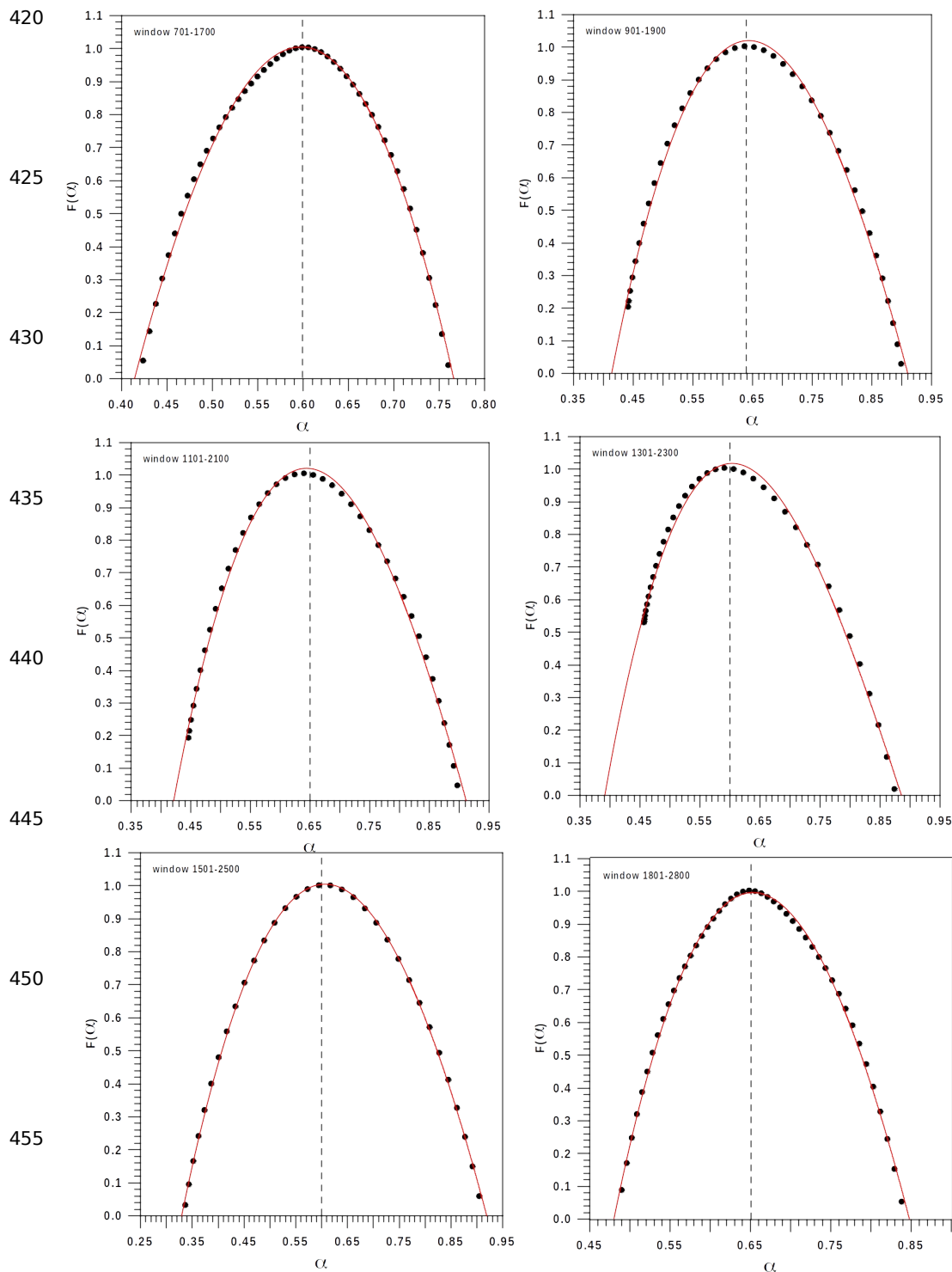380   **law (Monterrubio-Velasco et al., 2023).**

385

Figure 2: The analysed segment of energy emissions by means of multifractal theory, including the highest energy close to 108.4 J.

Figure 3: Six examples of multifractal spectrum, with ~~the two last moving windows including the maximum~~ ~~emission of energy~~ of Fig. 2. The ~~dashed line indicates the value of the central Hölder exponent~~ a0 for the maximum values of the spectrum.
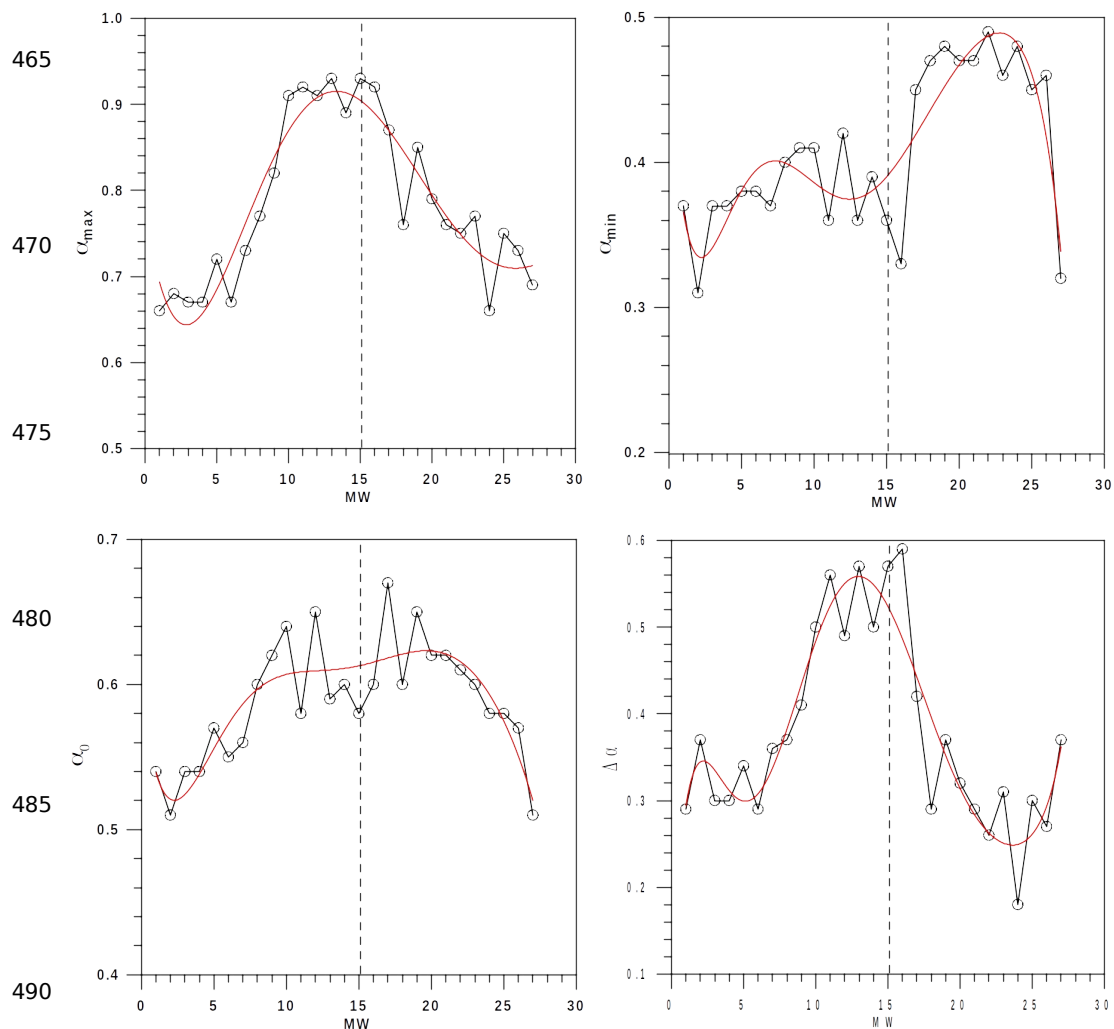
Figure 4: Evolution of the parameters amax, amin, a0 and W describing the structure of the multifractality along the 27 moving windows. Red lines describe the smooth evolution of these parameters by means of a polynomial of 5th degree. The dashed line indicates the MW = 15, which is the previous one to the highest emission.
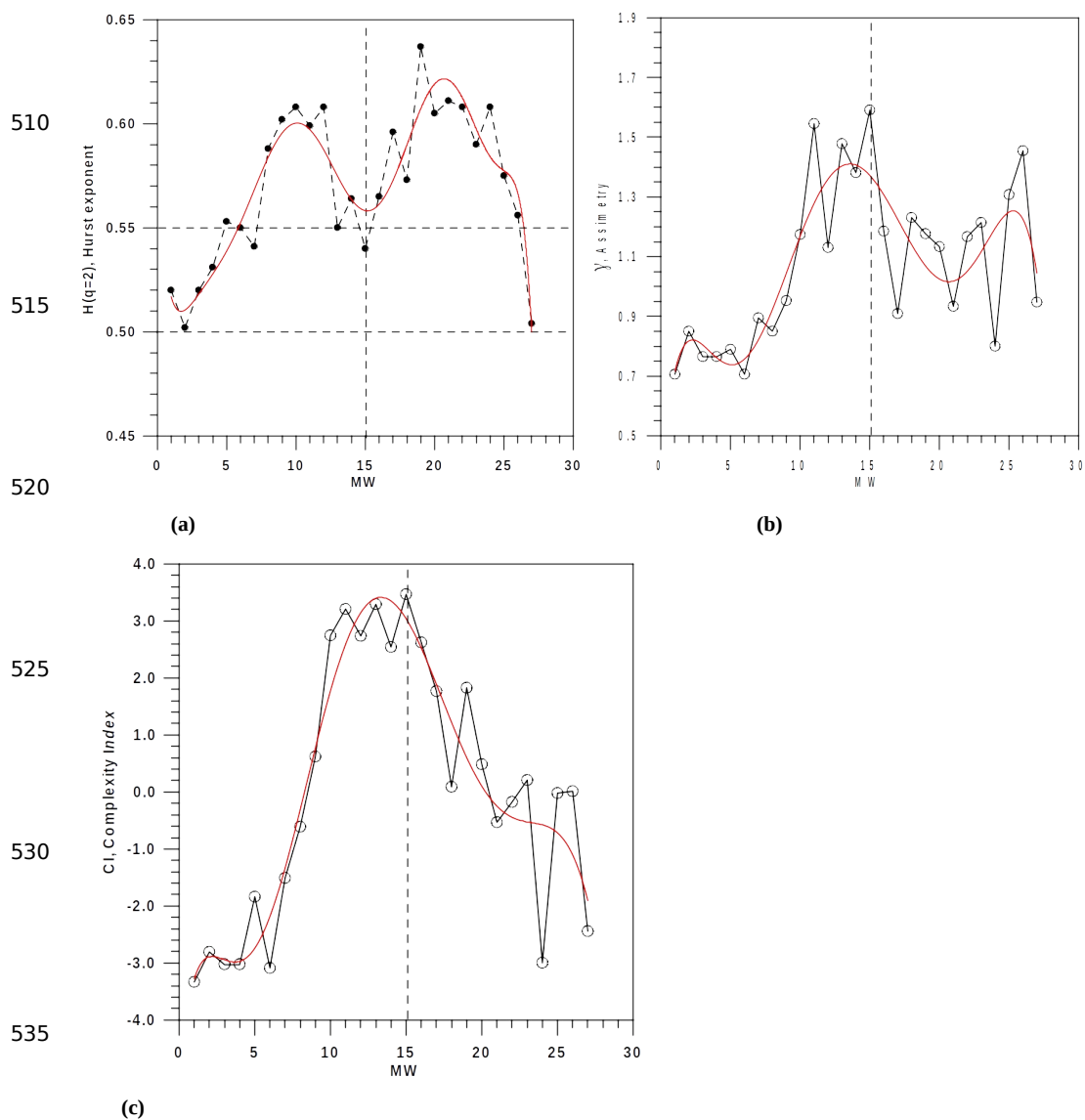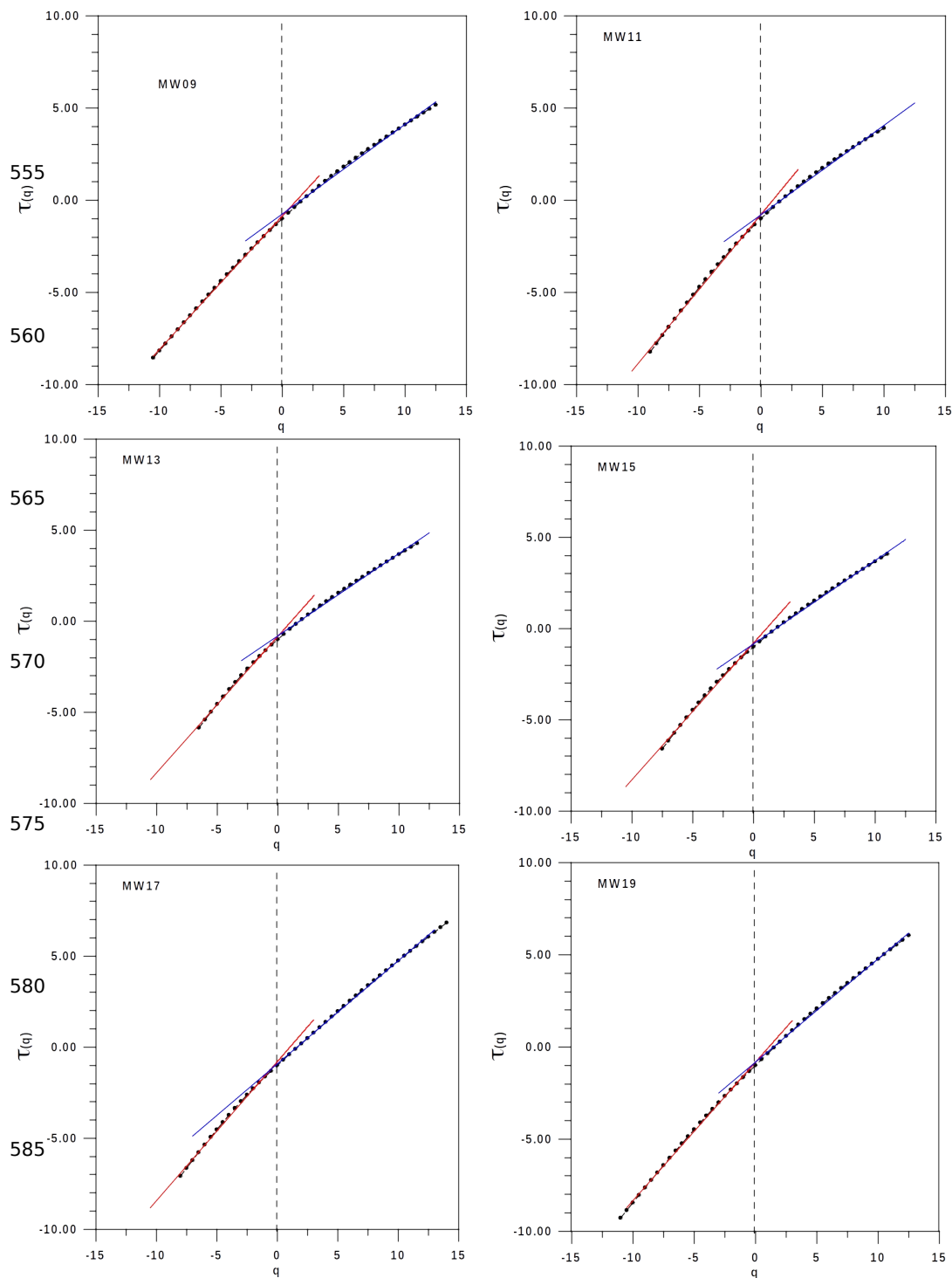
Figure 5: Evolution of a) the Hurst exponent, H(q=2), b) asymmetry, g, and c) complexity index, CI, of the multifractal structure. Red lines describe the smooth evolution of these parameters by means of a 5th degree polynomial. The dashed line indicates ~~the~~ MW = 15, ~~which is the previous one to~~ the highest emission.
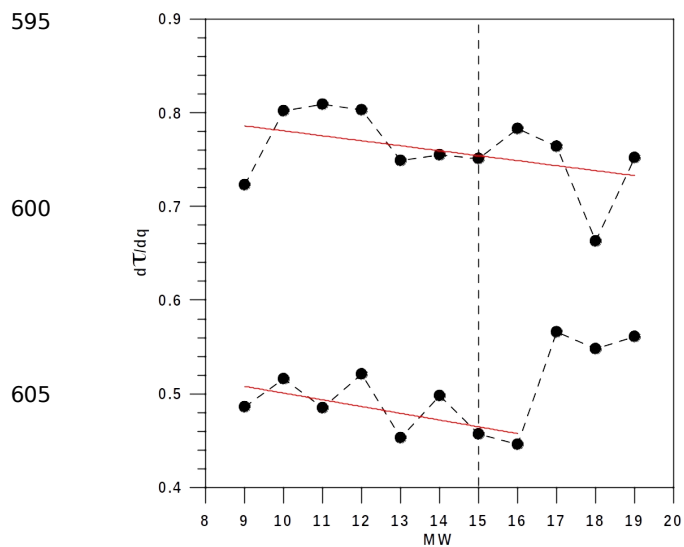
Nonlinear Processes
in Geophysics

Open Access

Discussions

EGU

Figure 6: Six examples of t(q) for MWs including (MW17,19) ~~and don't~~ including (MW9,11,13,15) the highest energy emission. The dashed line indicates the intersection of $\tau(q)$ for q = 0.

Nonlinear Processes
in Geophysics
Discussions

Open Access

EGU

Figure 7: Evolution of dτ/dQ for the moving windows 9 – 19, with the four last MW including the highest emission of energy. The dashed line indicates the MW = 15, which is the previous one to the highest emission.
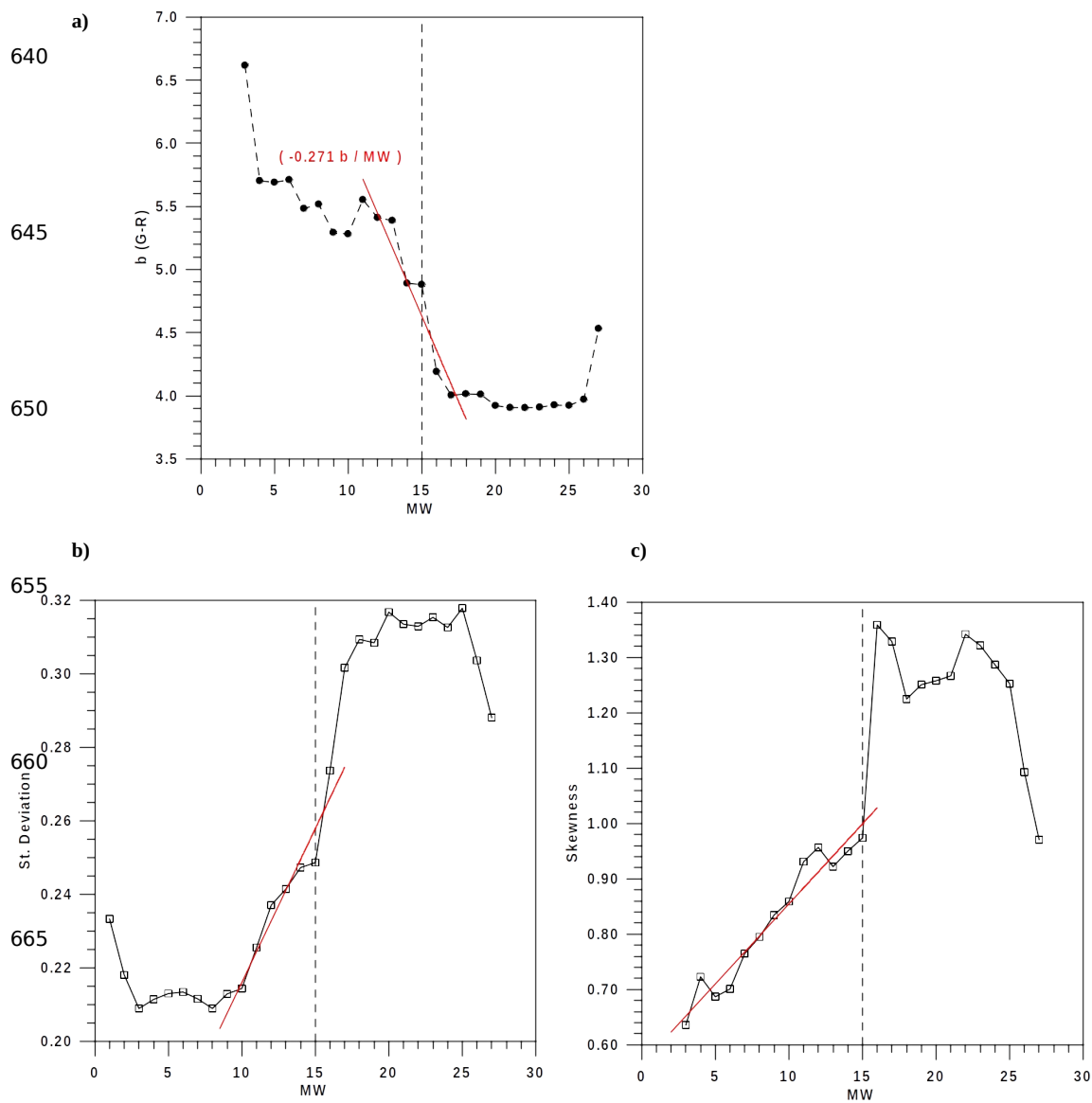
5

Nonlinear Processes
in Geophysics
Discussions

Figure 8: Evolution of a) the parameter b of Gutenberg-Richter, b) the standard deviation and c) the skewness of every MW. Red lines represent the linear trends corresponding to MWs close to the extreme emission and the dashed lines indicates the MW = 15 which is the previous one to the highest emission